Analysis and Design of Wing-Body Combinations at Subsonic and Supersonic Speeds

FRANK A. WOODWARD*
The Boeing Company, Seattle, Wash.

The method of aerodynamic influence coefficients has proved to be an effective tool for the analysis and design of wings, bodies, and wing-body combinations at supersonic speeds. This paper describes the extension of this method into the subsonic flow regime, and correlates the theory with experiment over a wide speed range. The method may be applied to the calculation of the pressures and forces acting on arbitrary wing-body combinations in steady flight, including aeroelastic effects, and to the design of wing camber surfaces in the presence of a body.

Nomenclature

A	=	aspect ratio
b	=	span
c	=	chord
C	=	aerodynamic coefficient
d	=	distance
f	=	singularity distribution function
F	=	distribution function
K	=	constant
l	=	body length
L	=	panel sweep
M	=	Mach number
r	=	radius
R_e	=	real part
u, v, w	=	perturbation velocities
U	=	freestream velocity
x, y, z	=	Cartesian coordinates
α	=	angle of attack
θ	=	angular coordinate, panel inclination
λ	=	taper ratio
Λ	=	leading edge sweep
ξ, η	=	integration variables
φ	=	velocity potential

Subscripts

D	=	drag
k	=	corner point
L	=	lift
M	=	moment
n	=	number
p	=	pressure
r	=	radial
α	=	per radian
θ	=	tangential
∞	=	freestream condition

Introduction

THE theory presented in this paper is a logical extension of the linearized supersonic flow theory reported in Refs. 1 and 2, and summarized in Ref. 3. The problem of calculating the surface pressures, forces, and moments acting on an arbitrary wing-body combination is solved by representing it by a system of source, doublet, and vortex singularities. The effects of body volume, incidence, and camber are simulated by line sources and doublets distributed along the body axis; the effects of wing thickness are represented by planar source distributions; and wing camber, twist, and incidence effects by planar vortex distributions. The interference effect of the wing on the body is provided by additional vortex distributions located on the body surface. The strengths of these singularities are determined such that the resulting flow is tangential to the surface at each control point.

The success of this method for analyzing supersonic flows led to an investigation directed toward extending it into the subsonic flow regime, since the linearized potential function is governed by the same partial differential equation in both cases. Further work revealed that a general solution valid for all Mach numbers could, in fact, be derived for each singularity. This unified approach for solving the linearized potential flow equation is the basis for the methods presented in this paper.

Aerodynamic Theory

A typical wing-body combination is illustrated in Fig. 1. The wing and the surface of the body in the interference region are subdivided into a large number of quadrilateral panels. These panels define the boundaries of planar singularities used to simulate the effects of wing lift, thickness, and wing-body interference. Additional line singularities located along the body axis are used to simulate the lift and volume effects of the body.

The singularities represent appropriate discontinuities in the u, v or w velocity components across the wing or body panels, or along the body axis. The potential function corresponding to each singularity must satisfy the Prandtl-Glauert equation

$$(1 - M^2)\varphi_{xx} + \varphi_{yy} + \varphi_{zz} = 0 \qquad (1)$$

Solutions of Eq. (1) may be written in integral form. For the line singularities,

$$\varphi_n = \int \frac{f_n(\xi)d\xi}{[(x-\xi)^2 + (1-M^2)r^2]^{1/2}} \qquad n = 1,2 \quad (2)$$

where $f_1 = -\xi$ for line sources and $f_2 = \sin\theta\xi(x-\xi)/r$ for line doublets. For the planar singularities

$$\varphi_n = \frac{K}{\pi}\iint \frac{f_n(\xi,\eta)d\xi d\eta}{\{(x-\xi)^2 + (1-M^2)[(y-\eta)^2 + z^2]\}^{1/2}} + \frac{1-K}{\pi}\iint \frac{z d\xi d\eta}{(y-\eta)^2 + z^2} \qquad n = 3,5 \quad (3)$$

Presented as Paper 68-55 at the AIAA 6th Aerospace Sciences Meeting, New York, January 22–24 1968; submitted January 11, 1968; revision received July 1, 1968. This research was supported in part by NASA Ames Research Center Contracts NAS2-2282 and NAS2-3719, and reported in NASA CR-69181 and NASA CR-73106, respectively.

* Research Specialist, Commercial Airplane Division; now Vice President, Aerophysics Research Corporation, Bellevue, Wash. Member AIAA.

where $K = 0.5$ for $M < 1$, $K = 1.0$ for $M > 1$, and $f_3 = -1$ for constant source distributions, $f_4 = L\eta - \xi$ for linearly varying source distributions, and $f_5 = z(x - \xi)/[(y - \eta)^2 + z^2]$ for constant pressure vortex distributions. The second term of Eq. (3) is included only for constant pressure vortex distributions.

The potential functions corresponding to each of these five singularity distributions may now be obtained by evaluating these integrals within the appropriate limits of integration. The perturbation velocity components are given by the partial derivatives of the potential function as follows:

$$u = \partial\varphi/\partial x \qquad v = \partial\varphi/\partial y \qquad w = \partial\varphi/\partial z \tag{4}$$

Line Source

The potential due to a finite line source of unit strength located along the x axis between $x = x_k$ and $x = l$ is obtained by integrating Eq. (2) for $n = 1$ between the limits $\xi = 0$ and $\xi = l$. In subsonic flow the integral may be evaluated directly, but for supersonic flow, the integral must be evaluated separately in each of the three regions bounded by the Mach cone from the origin and the Mach cone from the tail, as illustrated in Fig. 2. In either case, the final result may be written

$$\varphi_1 = R_e[d_1 - d_2 - x_1 \log(x_1 + d_1)/(x_2 + d_2)] \tag{5}$$

where

$$d_1 = [x_1^2 + (1 - M^2)r^2]^{1/2} \qquad x_1 = x - x_k$$
$$d_2 = [x_2^2 + (1 - M^2)r^2]^{1/2} \qquad x_2 = x - l$$

In subsonic flow, d_1 and d_2 may be interpreted as the distance from the origin or tail of the line source to the point $P'[x,(1 - M^2)r^{1/2}]$ in the Prandtl-Glauert coordinate system. In supersonic flow, both d_1 and d_2 are imaginary ahead of the Mach cone from the origin. Between the Mach cone from the origin and the Mach cone from the tail, d_1 is real but d_2 is imaginary. Behind the Mach cone from the tail, both d_1 and d_2 are real. The logarithmic term in Eq. (5) may be expressed as the difference of two functions as indicated below:

$$R_e \log(x_1 + d_1)/(x_2 + d_2) = F1(x_1) - F1(x_2) \tag{6}$$

where

$$F1(x) = R_e \log(x + d)/(|1 - M^2|)^{1/2}r$$

The function $F1$ can be expressed simply as an inverse hyperbolic sine in subsonic flow, or an inverse hyperbolic cosine in supersonic flow. The velocity components may now be obtained by differentiation. In cylindrical coordinates,

$$u = R_e[\log(x_2 + d_2)/(x_1 + d_1) + (l/d_2)]$$
$$v_r = (1/r)R_e[d_1 - (d_1^2 + x_1 l)/d_2] \tag{7}$$

In supersonic flow, these equations satisfy the boundary conditions of a circular cone at zero incidence.

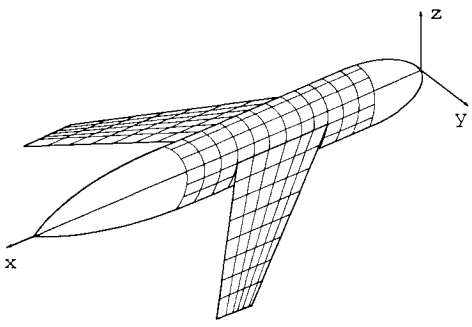

Fig. 1 Typical wing-body combination.

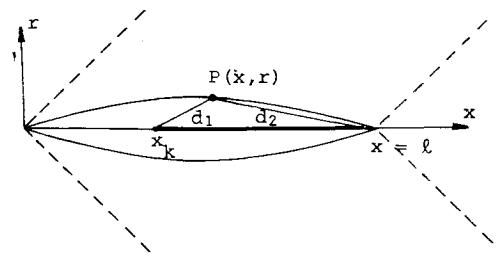

Fig. 2 Line source geometry.

Line Doublet

The potential due to a line doublet of unit strength located along the x axis is obtained by integrating Eq. (2) for $n = 2$ between the limits $\xi = 0$ and $\xi = l$. The potential function, valid for both subsonic and supersonic flows, is

$$\varphi_2 = \frac{\sin\theta}{2r} R_e\left[x_1(d_1 - d_2) - ld_2 + r^2(1 - M^2)\log\frac{x_1 + d_1}{x_2 + d_2}\right] \tag{8}$$

where d_1 and d_2 are defined as before and θ is measured from the x-y (horizontal) plane. The corresponding velocity components are

$$u_2 = (\sin\theta/r)\, R_e[d_1 - d_2 - x_2 l/d_2]$$
$$v_{r2} = (\sin\theta/2r^2)R_e\{x_1(d_2 - d_1) + ld_2 - (1 - M^2)r^2 \times [2l/d_2 - \log(x_1 + d_1)/(x_2 + d_2)]\} \tag{9}$$
$$v_{\theta 2} = (\cos\theta/2r^2)R_e[x_1(d_2 - d_1) + ld_2 - (1 - M^2)r^2 \times \log(x_1 + d_1)/(x_2 + d_2)]$$

Constant Source Distribution

The potential for a constant source distribution on a panel lying in the x-y plane is given by the first term of Eq. (3) for $n = 3$. The limits of integration are defined by the boundaries of the panel, as illustrated in Fig. 3.

If the equation of the leading edge is $\xi = L_1\eta$ where $L_1 = \tan\Lambda_1$, and the equation of the trailing edge is $\xi = c + L_2\eta$, it can be seen that the integral (3) may be considered as the sum of four integrals evaluated over semi-infinite triangular regions having origins at each of the four panel corners. That is, the potential at a point $P(x_p,y_p,z_p)$ is given by

$$\varphi_3(P) = \varphi_{31} - \varphi_{32} - \varphi_{33} + \varphi_{34} \tag{10}$$

where

$$\varphi_{3k} = \varphi_3(x_p - x_k, y_p - y_k, z_p) \qquad k = 1,4$$

and

$$x_1 = 0 \qquad x_2 = L_1 b \qquad x_3 = c \qquad x_4 = c + L_2 b$$
$$y_1 = 0 \qquad y_2 = b \qquad y_3 = 0 \qquad y_4 = b$$

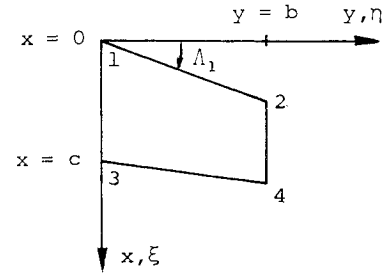

Fig. 3 Constant source panel geometry.

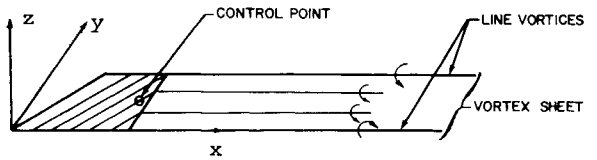

Fig. 4 Constant pressure panel with trailing vortex sheet.

The limits of the elementary integral φ_{3k} may now be defined

$$\varphi_{3k} = -\frac{K}{\pi}\int_0^{\eta_1} d\eta \times \int_{L\eta}^{\xi_1} \frac{d\xi}{\{(x-\xi)^2 + (1-M^2)[(y-\eta)^2+z^2]\}^{1/2}} \quad (11)$$

where

$$x = x_p - x_k \qquad y = y_p - y_k \qquad z = z_p$$

and ξ,η are measured from corner k. For subsonic flow $\xi_1 = \infty$ and $\eta_1 = \infty$. For supersonic flow

$$\xi_1 = x - \{(M^2-1)[(y-\eta)^2+z^2]\}^{1/2}$$

$$\eta_1 = \frac{Lx + (1-M^2)^{1/2}y - \{(M^2-1)[(x-Ly)^2 + (L^2+1-M^2)z^2]\}^{1/2}}{L^2+1-M^2} \quad (12)$$

The integral may now be evaluated, and the following result, valid for all Mach numbers, is obtained:

$$\varphi_{3k} = -(K/\pi)[yF1 + (x-Ly)F2 - zF3] \quad (13)$$

where

$$F1 = R_e\{\log (x+d)/[|1-M^2|r]^{1/2}\}$$

$$F2 = R_e\{\log (x'+d')/[|1-M^2|r']^{1/2}\}/(L^2+1-M^2)^{1/2}$$

$$F3 = R_e[\tan^{-1} zd/(Lr-xy)]$$

and

$$r = (y^2+z^2)^{1/2} \qquad d = [x^2 + (1-M^2)r^2]^{1/2}$$

$$x' = Lx + (1-M^2)y \qquad y' = x - Ly$$

$$r' = [(x-Ly)^2 + (L^2+1-M^2)z^2]$$

$$d' = [x'^2 + (1-M^2)r'^2]$$

It can be seen that the function $F2$ is proportional to $F1(x',d')$, and is obtained by applying a Lorentz transformation to the coordinate system. The line source is now located along the x' axis, which coincides with the panel leading edge.

The function $F2$ takes different forms, depending on the Mach number and the leading-edge sweep. For subsonic flows, $F2$ may be expressed as an inverse hyperbolic sine. For supersonic flows, $F2$ may be expressed as an inverse hyperbolic cosine if the leading edge is subsonic, or as an inverse cosine if the leading edge is supersonic. It should be noted that for supersonic flow, the Mach cone is invariant under a Lorentz transformation.

The function $F3$ provides the required discontinuity in the plane $z = 0$ corresponding to the specified singularity distribution. For example, in subsonic flow, $F3 = \pi$ for $x > Ly$ for $y > 0$, and for $x < Ly$ for $y < 0$. $F3 = 0$ everywhere else in the plane. For supersonic flow, $F3 = \pi$ only for $x > Ly$ and $y > 0$, and is zero elsewhere.

The velocity components for a constant source distribution are obtained by partial differentiation of Eq. (13). The results are

$$u_{3k} = -K\cdot F2/\pi \quad (14)$$

$$v_{3k} = K\cdot(L\cdot F2 - F1)/\pi \quad (15)$$

$$w_{3k} = K\cdot F3/\pi \quad (16)$$

It should be noted that

$$\varphi_{3k} = xu_{3k} + yv_{3k} + zw_{3k} \quad (17)$$

The velocity components induced at a point P by a finite panel may be obtained by superposition

$$u_3(P) = u_{31} - u_{32} - u_{33} + u_{34}$$

$$v_3(P) = v_{31} - v_{32} - v_{33} + v_{34} \quad (18)$$

$$w_3(P) = w_{31} - w_{32} - w_{33} + w_{34}$$

where the coordinate transformations are defined following Eq. (10). The constant source solution presented here for $M = 0$ is identical to that developed by Hess and Smith for incompressible potential flow in Ref. 4.

Linearly Varying Source Distribution

The potential for a linearly varying source distribution on a panel lying in the $x-y$ plane is given by the first term of Eq. (3) for $n = 4$. The potential function is chosen so that w equals zero along the panel leading edge. The limits of integration are defined by the panel boundaries as before.

The potential function corresponding to one corner element of the panel may now be evaluted. The result, valid for all Mach numbers, is

$$\varphi_{4k} = -(K/2\pi)\{[2xy + L(z^2-y^2)]\cdot F1 + [(x-Ly)^2 - L^2 + 1 - M^2]\cdot F2 - 2z(x-Ly)\cdot F3 - yd\} \quad (19)$$

where $F1$, $F2$, $F3$, and d are defined following Eq. (13). No new functional relationships are introduced in this solution, only the coefficients of the functions are changed.

The corresponding velocity components are obtained by partial differentiation of Eq. (19);

$$u_{4k} = -K[(x-Ly)\cdot F2 + yF1 - zF3]/\pi \quad (20)$$

$$v_{4k} = K[(x-Ly)\cdot(L\cdot F2 - F1) + d - z\cdot L\cdot F3]/\pi \quad (21)$$

$$w_{4k} = K\{(x-Ly)\cdot F3 - L\cdot F1 + z[(L^2+1-M^2)\cdot F2 - L\cdot F1]\}/\pi \quad (22)$$

In this case

$$\varphi_{4k} = (xu_{4k} + yv_{4k} + zw_{4k})/2 \quad (23)$$

The velocity components induced at a point P by a finite panel may be obtained by superposition, as indicated by Eq. (18).

Constant Pressure Vortex Distribution

The potential corresponding to a constant pressure difference across a panel lying in the x-y plane is given by Eq. (3) for $n = 5$. The limits of integration are defined by the panel boundaries as before.

The discontinuity in pressure coefficient is equivalent to a discontinuity in the axial velocity component u in the linearized theory. Since $C_p = -2u$,

$$\Delta C_p = C_{p_{lower}} - C_{p_{upper}} = -2\Delta u \quad (24)$$

The discontinuity in u will be used as the basic singularity in the following analysis.

The potential function corresponding to one corner element of a panel may now be evaluated. The result, valid for all Mach numbers, is

$$\varphi_{5k} = K\Delta u\{(x-Ly)\cdot(F3+F4) + z[(L^2+1-M^2)F2 - L(F1-F5)]\}/2\pi \quad (25)$$

where $F1$, $F2$, and $F3$ are defined following Eq. (13). Two

new functions are introduced in this solution,

$$F4 = \tan^{-1}(y/z) \quad \text{for } M < 1$$
$$= 0 \quad \text{for } M \geq 1 \tag{26}$$

and

$$F5 = \log(Lr/r') \quad \text{for } M \leq 1$$
$$= 0 \quad \text{for } M > 1 \tag{27}$$

The corresponding velocity components are obtained by partial differentiation of Eq. (25);

$$u_{5k} = K\Delta u(F3 + F4)/2\pi \tag{28}$$

$$v_{5k} = -K\Delta u[L\cdot(F3 + F4) - z\cdot F6]/2\pi \tag{29}$$

$$w_{5k} = K\Delta u[(L^2 + 1 - M^2)\cdot F2 - L\cdot(F1 - F5) - y\cdot F6]/2\pi \tag{30}$$

where

$$F6 = (x + d)/r^2 \quad \text{for } M \leq 1$$
$$= d/r^2 \quad \text{for } M > 1 \tag{31}$$

and

$$d = R_e[x^2 + (1 - M^2)r^2]^{1/2}$$

as before. For $M = 1$, it should be noted that

$$w_{5k} = \Delta u[L\cdot F5 - xy/r^2]/2\pi \quad \text{for } x > 0$$
$$= 0 \quad \text{for } x \geq 0 \tag{32}$$

since

$$F5 = L\cdot F2 - F1 \quad \text{for } M = 1$$

Again, it can be seen that a simple relationship exists between the potential function and the velocity components:

$$\varphi_{5k} = xu_{5k} + yv_{5k} + zw_{5k} \tag{33}$$

The velocity components induced at a point P by a finite panel may be obtained by superposition, as indicated by Eq. (18).

For the constant pressure singularities, the combined flow field for a finite panel is characterized by trailing line vortices from each side edge. If the panel is tapered, the trailing line vortices have unequal circulation, and the difference is made up by a trailing vortex sheet located between the two line vortices. On the panel itself, the circulation is distributed uniformly over the surface. The trailing vortex sheet is illustrated in Fig. 4.

At infinite distance behind the panel, the downwash along the panel centerline approaches a constant value independent of Mach number;

$$w_\infty = -2\Delta u/\pi A \tag{34}$$

where A = panel aspect ratio b/c.

It should be recognized that the constant pressure panel represents a highly cambered surface having infinite slopes on all edges, except those for which $L < (M^2 - 1)^{1/2}$ (supersonic edges in supersonic flow). As a result, the choice of the downwash control point is important if realistic lifting solutions are desired. The downwash control point chosen in this method is located at 95% of the local panel chord through the centroid. This control point location has been determined empirically by an extensive correlation of chordwise pressure distributions and lift curve slopes, for a variety of wing planforms at both subsonic and supersonic speeds. No theoretical argument has yet been developed to support this choice of control point.

Method of Analysis

The wing-body combination is represented by distributions of singularities, whose strengths are adjusted to satisfy the boundary conditions required by the geometry of the particular configuration. A typical wing-body combination is illustrated in Fig. 1. The wing, and the surface of the body in the wing-body interference region, is subdivided into a large number of small panels. Each panel defines an area over which a particular singularity strength is held constant. In order to simplify the analysis, the body panels are assumed to lie on the surface of a cylinder representing the mean surface of the body. The wing plane is assumed to be parallel to the body axis, and intersects the body along a line formed by the body panel edges. High or low wing configurations may be considered, but the effect of dihedral is not included. The wing sections may have arbitrary camber, twist, incidence, or thickness distributions, which are introduced as perturbations about the mean wing plane.

Associated with each panel and line singularity used to represent the configuration is a control point for matching the boundary conditions. The aerodynamic problem is formulated as a system of linear equations relating the velocity components normal to the surface at each control point to the unknown singularity strengths. The coefficients of this system of equations are computed in terms of the v and w velocity components given in the previous section, and stored as a matrix of aerodynamic influence coefficients. The details of this procedure are outlined in Ref. 1.

Two types of problems are considered. In the direct, or analysis, problem, the surface slopes at the control points are given, and the singularity strengths determined by inverting the aerodynamic matrix equations.

In the indirect, or design, problem, mixed boundary conditions are normally specified. For example, the slopes at the body control points and the pressure difference across the wing panels may be given. These types of problems may be solved by applying the techniques of matrix algebra to the system of linear equations. The wing optimization problem is a special case of the indirect problem, and is described in detail in Ref. 1.

Once the singularity strengths that satisfy all the boundary conditions are computed, the surface pressure distributions, lift, drag, and pitching moment on the wing and body may be obtained. The forces and moments are computed by integration of the surface pressures. Consequently, the leading-edge thrust associated with wings in subsonic flow, or subsonic leading-edge wings in supersonic flow, is not included in the drag calculation.

Results and Discussion

The application of the method to the analysis and design of wings, bodies, and wing-body combinations at supersonic speeds has been presented in Refs. 1, 2, and 3. The examples given below are chosen primarily to illustrate the application of the method to the analysis of subsonic flows, although some additional supersonic results are given to show the continuity of the method throughout the transonic regime.

Pressure Distribution on an Isolated Wing

The planform of the symmetrical, untwisted wing is shown in Fig. 5. The wing has an aspect ratio of 3, taper ratio 0.5, and quarter-chord sweepback of 45°. The NACA 65A010 section is defined normal to the quarter-chord line. The experimental pressure data for $M = 0.08$, $\alpha = 4°$, and $RN = 8 \times 10^6$ was obtained from Ref. 5 and is plotted as a function of chord for three spanwise stations in Fig. 6. These data are compared with the results of the present method calculated for $M = 0$. The agreement between the theory and the experiment is seen to be excellent over the entire wing, except in the immediate vicinity of the leading edge.

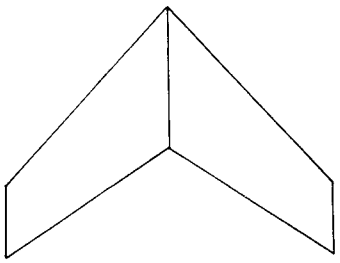

Fig. 5 Wing planform.

Lift-Curve Slopes of Isolated Wings

The lift-curve slopes of three aspect ratio 4 wings having 45° leading edge sweep are plotted as a function of Mach number in Fig. 7. The curves are conventional and agree with the predictions of other linearized theories over the entire Mach number range. It should be noted that the theoretical lift-curve slope for $M = 0$ agrees closely with the experimental values shown on pp. 96 and 97 of Ref. 6, for $\lambda = 0$ and 1.

Subsonic Wing-Body Combination at Zero Lift

A swept wing centrally mounted on an ellipsoidal body at zero incidence is chosen for this example. The geometry is illustrated in Fig. 8. The wing has an aspect ratio of 3, taper ratio $\frac{1}{3}$, and the leading edge is swept back 53.5°. It has a symmetrical RAE 101 airfoil 6% thick. The body is three times the length of the wing root chord and has a fineness ratio of 8. The pressure distribution on this wing-body combination at $M = 0$ is given by Hess and Smith in Fig. 37 of Ref. 4.

The body pressure distributions calculated by the present method are given in Fig. 8. Comparing these results with the isobars shown in Ref. 4, it can be seen that the present method predicts slightly lower peak negative pressures on the body in the wing-body interference region. Insufficient information can be obtained from the isobars to determine the peak positive pressure predicted immediately ahead and behind the wing leading and trailing edges on the body, however. The wing isobars from Ref. 4 have been interpolated and replotted on Fig. 9 as chordwise pressure distributions for three

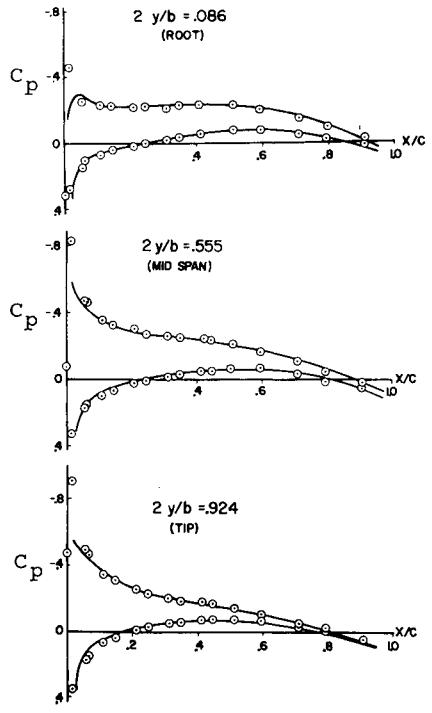

Fig. 6 Chordwise pressure distributions, $M = 0.08$, $\alpha = 4°$.

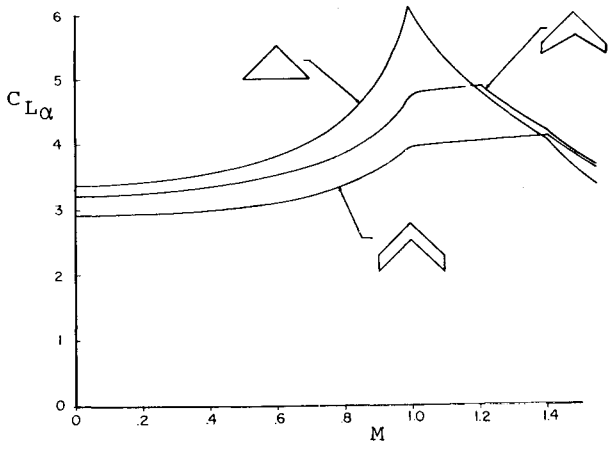

Fig. 7 Lift-curve slopes—aspect ratio 4 wings.

spanwise stations. The two methods agree exceptionally well in this example. It should be noted that Hess and Smith satisfy the flow boundary conditions on the surface of both the wing and body. The present method satisfies the body boundary conditions on the body surface, and the wing boundary conditions on the wing plane of symmetry. This linearization of the boundary conditions does not introduce appreciable error into the results for this 6% thick wing.

Transonic Wing-Body Combinations at Incidence

The wing-body combination selected for this example is illustrated on Fig. 10. The wing has an aspect ratio of 4, taper ratio 0.6, and a quarterchord sweepback of 45°. The wing has no twist, a symmetrical NACA 65A006 section parallel to the flow, and is centrally mounted on the body. The body has an over-all fineness ratio of 12, although an actual fineness ratio of 10 is obtained after the tail of the body is removed for sting attachment. The model was tested in the Langley 8-ft tunnel between $M = 0.6$–1.2, for a range of angle of attack and Reynolds number. Experimental pressure and force data for this configuration is given in Ref. 7.

The wing pressure data for $\alpha = 4°$ is plotted as a function of chord for three spanwise stations in Fig. 11. Data are presented for three Mach numbers and compared with the present theory. For $M = 0.6$, the flow is purely subsonic and the agreement between theory and experiment is excellent, except in the vicinity of the leading edge. For $M = 0.9$, the oncoming flow is subsonic, but local areas of supersonic flow have developed on the upper surface. The critical pressure coefficient, corresponding to a local Mach number of unity, is indicated by the dashed line on the figure. The present theory still shows acceptable agreement with experiment on the lower surface, where the pressure coefficient is subcritical,

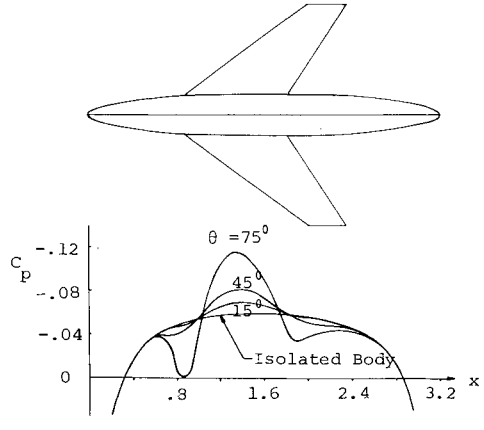

Fig. 8 Subsonic wing-body geometry, $M = 0$, $\alpha = 0$.

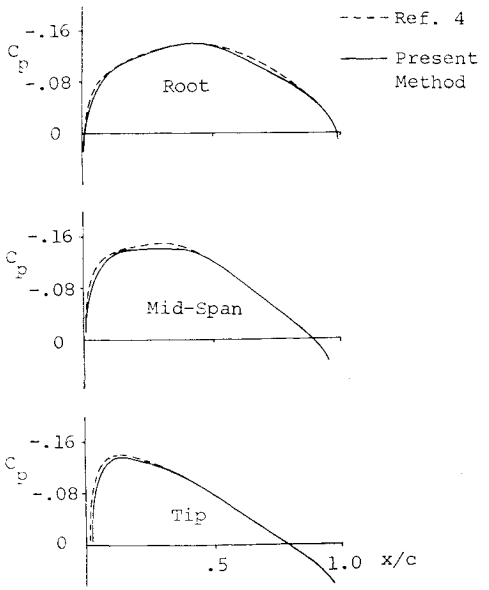

Fig. 9 Chordwise pressure distributions, $M = 0$, $\alpha = 0$.

but does not predict the upper surface pressure coefficient accurately in regions of supercritical flow. This breakdown in the theory in regions of supercritical flow is to be expected, as the regions of influence of the individual singularities are changed significantly in the transition from subsonic to local supersonic flow. However, the theory gives useful information on the approximate extent of the region of supercritical flow, though it does not give acceptable results for the magnitude of the pressure coefficients in this region. For $M = 1.2$ the flow is purely supersonic, and the agreement between the theory and experiment is again acceptable, except near the leading edge. This example again shows the need for a leading-edge pressure correction to linearized theory that is valid for swept wings in subsonic compressible flows, and for subsonic leading-edge wings in supersonic flows.

The body pressure data for $\alpha = 4°$ is plotted as a function of the distance from the nose for four meridian lines located

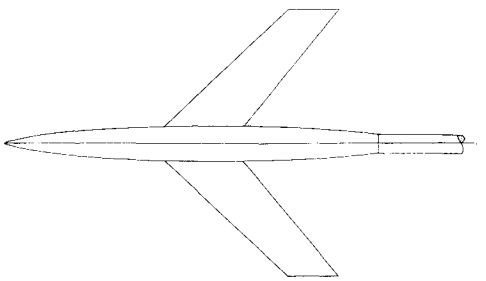

Fig. 10 Transonic wing-body geometry.

15°, 75°, 105°, and 165° from the top of the body. The data are shown in Fig. 12. The agreement between the theory and experiment is acceptable for purely subsonic flow, $M = 0.6$, except in the immediate vicinity of the wing leading edge. For $M = 0.9$, the agreement is again satisfactory, except in regions where the local velocity is supersonic. The critical pressure coefficient level is indicated by the dashed line. Finally, for $M = 1.2$, the theoretical predictions also show acceptable agreement with the experimental data.

Applications

In addition to the determination of the pressures, forces, and moments acting on arbitrary wing-body combinations at subsonic and supersonic speeds, the method has important applications in the solution of wing design problems. It may be used to determine the wing camber, twist, and thickness distribution which gives a specified upper surface pressure distribution in the presence of the body. This technique is useful in the design of wing-body intersections that avoid undesirable interference effects and can lead to increases in the cruising Mach number of subsonic transports. Similarly, the design of the wing camber and twist for minimum drag under given constraints of lift and pitching moment can improve the over-all efficiency of supersonic transports

The method also can be applied effectively to the solution of aeroelastic problems at both subsonic and supersonic speeds. A linear relationship is established between the aerodynamic forces acting on the wing panels and the cor-

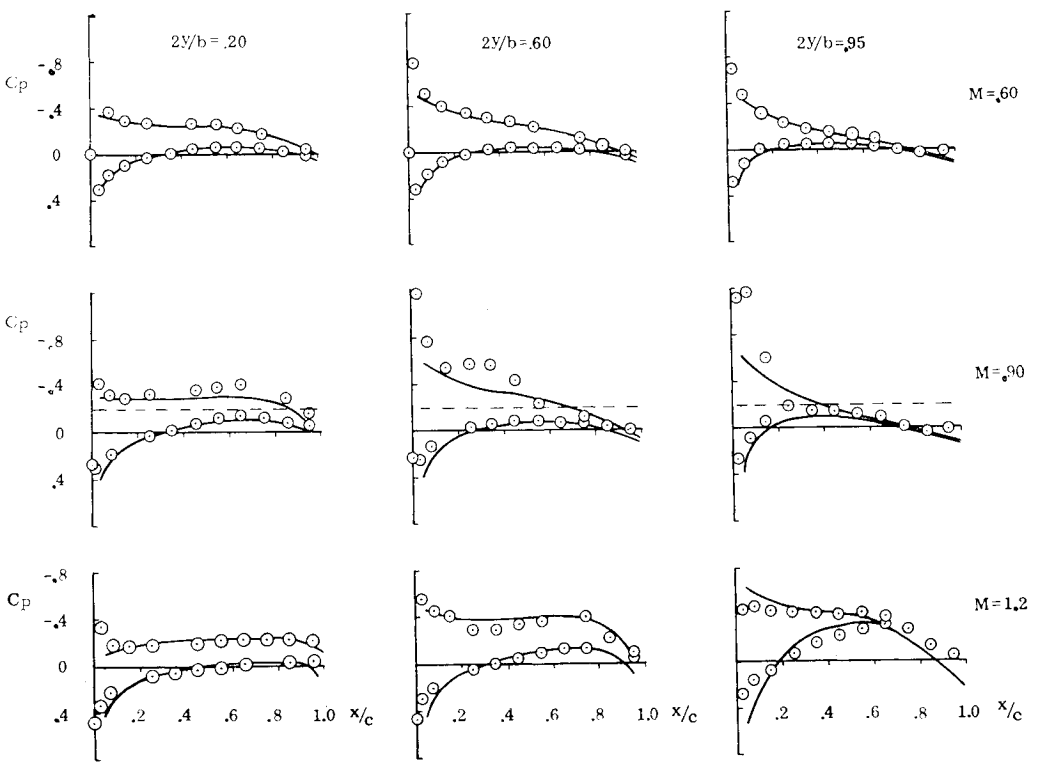

Fig. 11 Wing pressure distributions, $\alpha = 4°$.

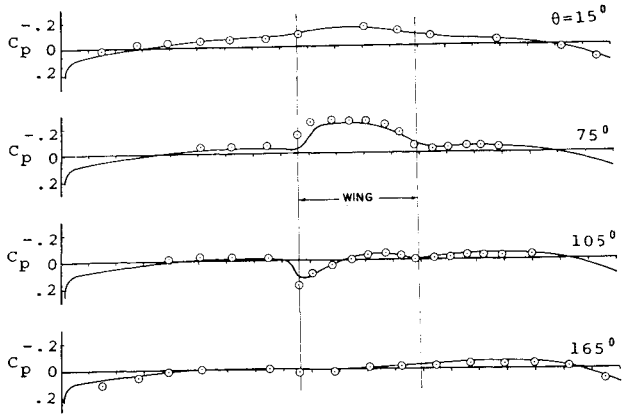

a) $M = 0.6$

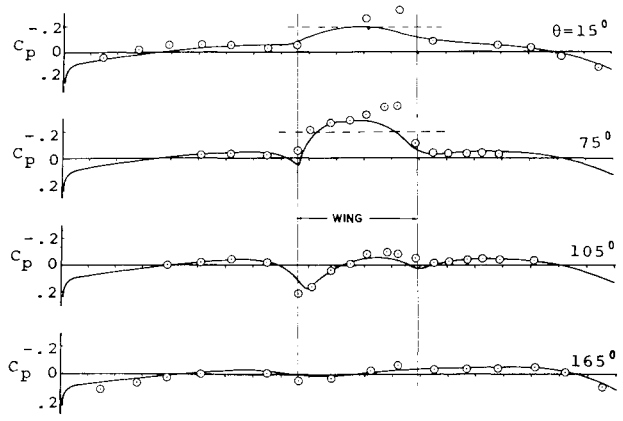

b) $M = 0.9$

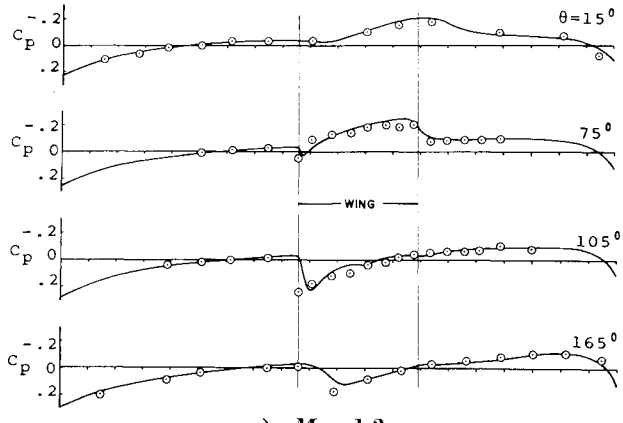

c) $M = 1.2$

Fig. 12 Body pressure distributions, $\alpha = 4°$.

responding structural deflections. The resulting system of equations may be solved directly to obtain the elastic airload distributions and the deformed structural shape. This approach may be extended to derive simple, explicit expressions for the rigid and elastic longitudinal stability derivatives of arbitrary configurations. An example is presented in Ref. 8 which compares theoretical stability derivative estimates with experimental data.

Conclusions

A highly versatile method for the analysis and design of wings, bodies, and wing-body combinations in subsonic and supersonic flows has been described. Acceptable agreement between the theory and experiment has been demonstrated over a wide range of Mach numbers. The method may be applied to the calculation of the pressures, forces, and moments acting on arbitrary wing-body combinations in steady flight, including aeroelastic effects, and to the design of wing camber surfaces in the presence of a body.

References

[1] Woodward, F. A., Tinoco, E. N., and Larsen, J. W., "Analysis and Design of Supersonic Wing-Body Combinations, Including Flow Properties in the Near Field—Part I—Theory and Application," CR-73106, Aug. 1967, NASA.

[2] Woodward, F. A. and Larsen, J. W., "A Method of Optimizing Camber Surfaces for Wing-Body Combinations at Supersonic Speeds—Theory and Application," Document D6-10741—Pt. 1, Sept. 1965, The Boeing Co.; also available as NASA CR-69181.

[3] Carmichael, R. L. and Woodward, F. A., "An Integrated Approach to the Analysis and Design of Wings and Wing-Body Combinations in Supersonic Flow," TN D-3685, Oct. 1966, NASA.

[4] Hess, J. L. and Smith, A. M. O., "Calculation of Non-Lifting Potential Flow About Arbitrary Three-Dimensional Bodies," Rept. E. S. 40622, 1962, Douglas Aircraft Co.

[5] Kolbe, C. D. and Boltz, F. W., "The Forces and Pressure Distribution at Subsonic Speeds on a Plane Wing Having 45° of Sweepback, an Aspect Ratio of 3, and a Taper Ratio of .5," RM A51G31, Oct. 1951, NACA.

[6] Jones, R. T. and Cohen, D., *High Speed Wing Theory*, Princeton University Press, 1960.

[7] Loving, D. L. and Estabrooks, B. B., "Transonic-Wing Investigation in the Langley 8-Foot High-Speed Tunnel at High Subsonic Mach Numbers and at a Mach Number of 1.2—Analysis of Pressure Distribution of Wing-Fuselage Configuration Having a Wing of 45° Sweepback, Aspect Ratio 4, Taper Ratio .6 and NACA 65A006 Airfoil Section," RML51F07, Sept. 1951, NACA.

[8] Roskam, J., Holgate, T., and Shimizu, G., "Development and Use of Elastic Wind-Tunnel Models in Predicting Longitudinal Stability Derivatives of Elastic Airplanes," Paper 68-56, Jan. 1968, AIAA; also *Journal of Aircraft*, Vol. 5, No. 6, Nov.–Dec. 1968, pp. 543–550.